Journal of Signal Processing, Vol.21, No.5, pp.211-224, September 2017

PAPER

Development of Quasi-Shift-Invariant Complex Discrete Wavelet Transform

Makoto Kobayashi[1] and Kazushi Nakano[2]

[1] Water Works Bureau, City of Yokohama, 23 Yamashita-cho, Naka-ku, Yokohama, Kanagawa 231-0023, Japan
[2] The University of Electro-Communications, 1-5-1 Chofugaoka, Chofu-shi, Tokyo 182-8585, Japan

E-mail: [1]ma56-kobayashi@city.yokohama.jp, [2]nakano@office.uec.ac.jp

Abstract **The downsampling of a discrete wavelet transform (DWT) has a side effect of the lack of shift-invariance. There are two main solutions for this effect: one is the stationary wavelet transform (SWT), which does not apply downsampling. The other is the complex DWT (CDWT), which uses dual multiresolution analysis (MRA). We choose the CDWT as a target of research. It is well known that wavelet functions become Hilbert transform pairs if the low-pass filters (LPFs) on the reconstruction side have half-sample shifts. In this paper, we propose a quasi-shift-invariant (QSI) CDWT for bi-/orthogonal wavelets as a new CDWT. We report three new works (W1-W3) on it: (W1) we generalized the condition of Hilbert transform pairs and employed a complex wavelet function as a conjugate analytical signal. (W2) We defined a structure that achieves shift-invariance. The structure requires half-sample delays between the inputs of real and imaginary parts. (W3) We proposed an implementation of the QSI-CDWT and confirmed that our method has higher shift-invariance than the conventional CDWT. However, two problems (P1, P2) remain unsolved: (P1) our method requires more resources, such as memory and calculation time, than the conventional CDWT. (P2) Our theory cannot make all packets shift-invariant in a classical wavelet packet transform tree.**

Keywords: shift-invariance, orthogonal wavelet, bi-orthogonal wavelet, complex discrete wavelet transform

1. Introduction

The Fourier transform [1] is a technique that transforms time-domain signals to frequency-domain ones. There is a fast computation algorithm [2] for the Fourier transform that is widely used in the scientific and engineering fields. Wavelet transforms [3–5] came into existance toward the end of the 20th century. They are a time-frequency analysis tool similar to the short-time Fourier transform (STFT) [5]. The STFT requires parameters of the window function to be adjusted depending on the frequency range. Although this enables a precise analysis, the users require expert skills. The wavelet transform gives the relationship between the window function and the intended frequency range. Without the labor required for the STFT, it enables an adequate analysis with reasonable accuracy.

The discrete wavelet transform (DWT) [3–5] is one of the wavelet transforms. The DWT targets discrete-time signals, and is the same as the two-channel filter bank [6, 7]. The DWT using a bi-/orthogonal wavelet corresponds to a bi-/orthogonal filter bank, respectively, and both can reconstruct a signal from decomposed signals correctly. In multiresolution analysis (MRA) [8] of the DWT, the output signal retains every even-indexed sample of the source signal. This operation is called downsampling [9].

The DWT has the problem known as a *lack of shift-invariance* [10] or a lack of translation-invariance. This means that the reconstructed signal or the energy of a DWT output varies depending on the time shifts of the input signal. Shift-invariance is a very important property for some applications such as change detection and denoising. The downsampling causes the lack of shift-invariance [10]. Many proposed methods have been reported for overcoming the problem, including the undecimated wavelet transform (stationary wavelet transform; SWT) [11] and the complex DWT (CDWT) [12, 13], by constructing a Hilbert transform pair of wavelet functions [14]. In this paper, we choose the CDWT as a target of research.

This paper is organized as follows. Section 2 summarizes some definitions and already known facts. We describe our proposed CDWT in Sect.3, which is the novelty of this paper. Section 4 reports three experiments using our CDWT and shows the results. Finally, we conclude the paper in Sect.5.

We use the notation $\mathbb{N} = \{1, 2, \ldots\}$, $\mathbb{N}_0 = \{0\} \cup \mathbb{N}$, $\mathbb{Z} = \{0, \pm1, \pm2, \ldots\}$ and $\mathbb{B} = \{0, 1\}$. We denote $\mathcal{F}[\cdot]$ as the

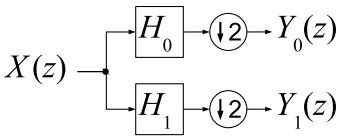

Fig. 1 Illustration of DWT in block diagram representation

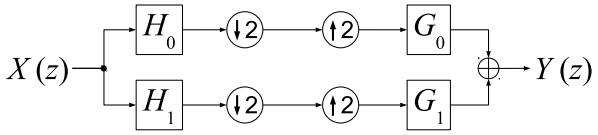

Fig. 2 Illustration of two-channel filter bank in block diagram representation

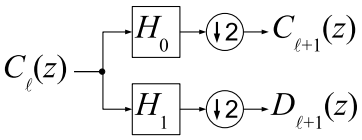

Fig. 3 Illustration of MRA using DWT in block diagram representation. ℓ for the original input is zero

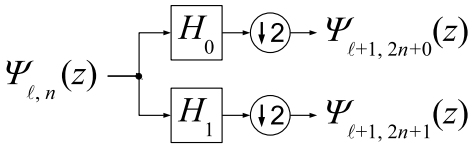

Fig. 4 Illustration of WPT in block diagram representation. ℓ and n for the original input are zero

Fourier transform and $\mathcal{H}[\cdot]$ as the Hilbert transform. $\mathcal{Z}[\cdot]$ and $\mathcal{Z}^{-1}[\cdot]$ are the Z-transform and inverse Z-transform, respectively. They are

$$S(z) = \mathcal{Z}[s] = \sum_{n\in\mathbb{Z}} s[n] z^{-n} \tag{1}$$

$$s[n] = \mathcal{Z}^{-1}[S] = \frac{1}{2\pi \mathrm{j}} \oint_C S(z) z^{n-1} \mathrm{d}z \tag{2}$$

where C is the appropriate region of convergence (ROC).

2. Previous Research

In this section, we summarize previous research and show the lack of shift-invariance.

2.1 Discrete wavelet transform

In this subsection, we summarize previous findings [3–5] simply.

Figure 1 shows one-level decomposition of a DWT in a block diagram representation, which is the same as the two-channel filter bank [7]. The downsampler and the upsampler are respectively expressed in the Z-domain [7] as follows:

$$Y(z) = \frac{1}{2} X\left(z^{\frac{1}{2}}\right) + \frac{1}{2} X\left(-z^{\frac{1}{2}}\right) \tag{3}$$

$$Y(z) = X\left(z^2\right) \tag{4}$$

where X is the input and Y is the output, respectively. The first term of Eq. (3) is a signal component and the second one is an aliasing component. If an appropriate low-pass filter (LPF) is applied before the downsampling, the filter suppresses the aliasing component. Figure 2 shows a two-channel filter bank. The filter bank satisfies the following two equations for perfect reconstruction:

$$H_0(-z) G_0(z) + H_1(-z) G_1(z) = 0 \tag{5}$$

$$H_0(z) G_0(z) + H_1(z) G_1(z) = 2z^{-M} \tag{6}$$

where $M \in \mathbb{N}_0$. We use H_0 as the LPF of the decomposition side. H_1 is the high-pass filter (HPF) of the decomposition side. G_0 and G_1 are the synthesis filters corresponding to H_0 and H_1, respectively. The above equations are equivalent to

$$Y(z) = z^{-M} X(z) \tag{7}$$

The conjugate quadrature filter (CQF) bank [6, 7] is one of the filter banks using FIR filters. It guarantees perfect reconstruction. The DWT and the inverse DWT using orthogonal wavelets are the same as the CQF bank. The filters H_1, G_0 and G_1 of the CQF bank are subordinate to H_0 as follows:

$$H_1(z) = -z^{-(L-1)} H_0\left(-z^{-1}\right) \tag{8}$$

$$G_0(z) = H_1(-z) \tag{9}$$

$$G_1(z) = -H_0(-z) \tag{10}$$

where $L = 2k$ ($k \in \mathbb{N}$) is the length of the impulse response of H_0. If $L = 2k + 1$, then we pad one sample with a value of 0 at the end of H_0 to make L an even number. If we build a system regardless of the causality, L can be arbitrarily assigned by appropriately selecting a positive value. We substitute Eqs. (8), (9) and (10) into Eq. (6) and obtain $M = L - 1$ and

$$|H_0(z)|^2 + |H_0(-z)|^2 = 2 \tag{11}$$

Equation (11) denotes the *power-complementary* property of the CQF bank.

The MRA [8] consists of some DWTs as shown in Fig.3. Each low-pass output is regarded as a new input. The system finely divides lower-frequency bands and roughly divides higher-frequency bands. The wavelet packet transform (WPT) [15] is a solution to improve

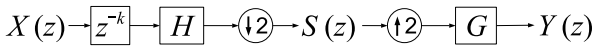

Fig. 5 Illustration used to explain the lack of shift-invariance

the higher-frequency resolution. Figure 4 shows that the WPT recursively uses the previous level's outputs as new inputs. The output of each channel is called the *packet*. Let us denote the packet by $\Psi_{\ell,n}$, where $\ell \in \mathbb{N}_0$ is the level and $n \in \mathbb{N}_0$ is the index of the channels. The output $\Psi_{\ell+1,2n+i}$ is formulated by using Eq. (3) as

$$\Psi_{\ell+1,2n+i}(z) = \frac{1}{2}H_i\left(z^{\frac{1}{2}}\right)\Psi_{\ell,n}\left(z^{\frac{1}{2}}\right) + \frac{1}{2}H_i\left(-z^{\frac{1}{2}}\right)\Psi_{\ell,n}\left(-z^{\frac{1}{2}}\right) \tag{12}$$

where $i \in \mathbb{B}$.

The CDWT [12] consists of two filter banks using the Hilbert transform [16] pair of wavelets [12, 13]. Two wavelets of the filter banks are ψ^{R} and ψ^{I}, respectively, where $\cdot^{\mathrm{R}}$ denotes the real part, $\cdot^{\mathrm{I}}$ denotes the imaginary part. The principle of the CDWT is based on the following theorem:

Theorem 1 (Hilbert transform pairs of wavelet bases) ψ^{I} is the Hilbert transform of ψ^{R} if G_0^{R} and G_0^{I} are the LPFs of the reconstruction side of two CQF banks and

$$G_0^{\mathrm{I}}(z) = z^{-\frac{1}{2}}G_0^{\mathrm{R}}(z) \tag{13}$$

Proof See [14]. □

The lifting scheme [17–19] is able to calculate the DWT sequentially. It has two methods of calculation: *in-place* and *sequential calculation*. The in-place calculation is an alternative way to calculate the circular convolution.

2.2 Lack of shift-invariance

In this subsection, we will clarify the definition of the shift-invariance.

Figure 5 shows the decomposition and the reconstruction of a signal with $k(\in \mathbb{Z})$-sample shifts. The pair (H, G) is a decomposition filter H and a reconstruction filter G corresponding to H, for example, (H_0, G_0) or (H_1, G_1) of the CQF bank. S is represented as

$$S(z) = \frac{1}{2}H\left(z^{\frac{1}{2}}\right)X\left(z^{\frac{1}{2}}\right)\left\{z^{\frac{1}{2}}\right\}^{-k} + \frac{1}{2}H\left(-z^{\frac{1}{2}}\right)X\left(-z^{\frac{1}{2}}\right)\left\{-z^{\frac{1}{2}}\right\}^{-k} \tag{14}$$

If $\mathcal{Z}^{-1}[S] = s$,

$$s[n] = 2\mathcal{Z}^{-1}[H(z)X(z)][2n-k] \tag{15}$$

where the calculation process is given in Appendix A. s is a time-varying signal depending on the value of k. The sampling points depend on whether k is an even or odd number. The reconstructed signal Y is

$$Y(z) = G(z)S\left(z^2\right) \tag{16}$$

which we can rewrite as

$$Y(z) = \frac{1}{2}G(z)z^{-k}\mathcal{Z}\left[\rho[n] + (-1)^{n+k}\rho[n]\right] \tag{17}$$

where $H(z)X(z) = \mathcal{Z}[\rho]$. The calculation process is given in Appendix B. Y is also a time-varying signal depending on k. This varying feature is the *lack of shift-invariance*.

3. Quasi-Shift-Invariant Discrete Wavelet Transform

We propose a new CDWT; the quasi-shift-invariant (QSI) CDWT. Here we show the principle and implementation of the QSI-CDWT.

3.1 Easing condition on Hilbert transform pairs

The previous research [14] showed that the wavelet function becomes $\psi^{\mathrm{R}} + \mathrm{j}\mathcal{H}\left[\psi^{\mathrm{R}}\right]$ if Eq. (13) is satisfied. We generalize Eq. (5) of [14] as

$$\theta(\omega) = \frac{\lambda\omega}{2} \tag{18}$$

where $\lambda \in \{\pm 1\}$. We rewrite Eq. (13) as

$$G_0^{\mathrm{I}}(z) = z^{-\frac{\lambda}{2}}G_0^{\mathrm{R}}(z) \tag{19}$$

By using Eqs. (8) and (9), we obtain

$$H_0^{\mathrm{I}}(z) = z^{\frac{\lambda}{2}}H_0^{\mathrm{R}}(z) \tag{20}$$

The $\lambda = 1$ case provides the Hilbert transform pair of wavelet functions. We summarize the discussion using λ in Appendix C. The complex wavelet function ψ becomes

$$\begin{aligned}\hat{\psi}(\omega) &= \mathcal{F}\left[\psi^{\mathrm{R}}(t) + \lambda\,\mathrm{j}\,\mathcal{H}\left[\psi^{\mathrm{R}}\right](t)\right] \\ &= \hat{\psi}^{\mathrm{R}}(\omega) + \lambda\,\mathrm{j}\,\mathcal{F}\left[\frac{1}{\pi t}\right]\hat{\psi}^{\mathrm{R}}(\omega) \\ &= \hat{\psi}^{\mathrm{R}}(\omega)\{1 + \lambda\,\mathrm{sgn}[\omega]\}\end{aligned}$$

If $\lambda = 1$, then the wavelet function becomes an analytical signal with only positive-frequency components. However, the $\lambda = -1$ case provides a wavelet function with only negative-frequency components. It also gets an orthogonal relationship between the real and imaginary parts. In this paper, by using λ, we ease the condition on the Hilbert transform pairs of the wavelet function for shift-invariance.

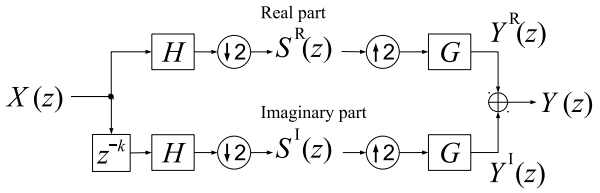

Fig. 6 Illustration of shift-invariant structure

3.2 Principle of shift-invariance

Many conventional CDWTs are based on Theorem 1. We will add a new condition for the conventional CDWT, and show that the condition leads to the shift-invariant structure that we will define.

Theorem 2 (shift-invariant structure) As shown in Fig.6, if $k = 2m + 1$ ($m \in \mathbb{N}_0$), then $Y^{\mathrm{R}} + Y^{\mathrm{I}}$ retains HX perfectly.

Proof S^{R} and S^{I} retain the samples of HX perfectly if $k = 2m + 1$, which is the same logic as in Eq. (15). As shown in Eq. (17), we obtain

$$Y^{\mathrm{R}}(z) = \frac{1}{2} G(z) z^{-k} \mathcal{Z}[\rho[n] + (-1)^n \rho[n]] \tag{21}$$

$$Y^{\mathrm{I}}(z) = \frac{1}{2} G(z) z^{-k} \mathcal{Z}\left[\rho[n] + (-1)^{n+k} \rho[n]\right] \tag{22}$$

where $H(z) X(z) = \mathcal{Z}[\rho]$. The following result is obtained through the linearity of z-transforms:

$$\begin{aligned} & Y^{\mathrm{R}}(z) + Y^{\mathrm{I}}(z) \\ &= \frac{1}{2} G(z) z^{-k} \mathcal{Z}\left[2\rho[n] + (-1)^n \rho[n] + (-1)^{n+k} \rho[n]\right] \\ &= \frac{1}{2} G(z) z^{-k} \mathcal{Z}[2\rho[n]] \\ &= G(z) z^{-k} H(z) X(z) \end{aligned}$$

where $k = 2m + 1$. □

We define the *shift-invariant structure* as follows:

Definition 1 (shift-invariant structure) We call the structure shown in Fig.6 the *shift-invariant structure*, if the twofold channel applies the same process except the time delay of $k = 2m + 1$ ($m \in \mathbb{Z}$).

We summarize the following important points about the structure:

- The shift-invariant structure is a mechanism for one channel, for example, only on the LPF side or only on the HPF side.
- The difference between real and imaginary parts is the time delay before decimation.
- We use the same filters in both parts.

When using the CQF bank, one filter can represent another filter by itself as shown in Eqs. (8), (9) and (10). This implies that we can theoretically use the same filter at each decimation of the real and imaginary parts. In addition, by giving a time delay to inputs, we can verify the shift-invariance of the shift-invariant structure.

We set the time delay β between a real input $\Psi^{\mathrm{R}}_{\ell,n}$ and an imaginary input $\Psi^{\mathrm{I}}_{\ell,n}$ as

$$\Psi^{\mathrm{I}}_{\ell,n}(z) = z^{-\beta} \Psi^{\mathrm{R}}_{\ell,n}(z) \tag{23}$$

By using Eq. (12), each output is written as

$$\psi^{\mathrm{R}}_{\ell+1,2n+0}[m] = 2\mathcal{Z}^{-1}[\varrho_0(z)][2m] \tag{24}$$

$$\psi^{\mathrm{I}}_{\ell+1,2n+0}[m] = 2\mathcal{Z}^{-1}[\varrho_0(z)]\left[2m - \beta + \frac{\lambda}{2}\right] \tag{25}$$

$$\psi^{\mathrm{R}}_{\ell+1,2n+1}[m] = 2\mathcal{Z}^{-1}[\varrho_1(z)][2m] \tag{26}$$

$$\psi^{\mathrm{I}}_{\ell+1,2n+1}[m] = 2\mathcal{Z}^{-1}[-\lambda \mathrm{j}\, \varrho_1(z)]\left[2m - \beta - \frac{\lambda}{2}\right] \tag{27}$$

where $m \in \mathbb{Z}$ and $\varrho_i(z) = H^{\mathrm{R}}_i(z) \Psi^{\mathrm{R}}_{\ell,n}(z)$. Equation (8) is not used except for in Eq. (27). Note that the relation between H^{R}_1 and H^{I}_1 is derived from Eqs. (8) and (20) as

$$\begin{aligned} H^{\mathrm{I}}_1(z) &= -z^{-(L-1)} H^{\mathrm{I}}_0\left(-z^{-1}\right) \\ &= -z^{L-1}\left(-z^{-1}\right)^{\frac{\lambda}{2}} H^{\mathrm{R}}_0\left(-z^{-1}\right) \\ &= \left(-z^{-1}\right)^{\frac{\lambda}{2}} H^{\mathrm{R}}_1(z) \\ &= \left(\mathrm{j}\, z^{\frac{1}{2}}\right)^{-\lambda} H^{\mathrm{R}}_1(z) \\ &= -\lambda \mathrm{j}\, z^{-\frac{\lambda}{2}} H^{\mathrm{R}}_1(z) \end{aligned}$$

LPF side If an appropriate β is choosen, Eqs. (24) and (25) eliminate the downsampling effect of $H^{\mathrm{R}}_0 \Psi^{\mathrm{R}}_{\ell,n}$. We can define such a β as

$$\beta = 2u + 1 + \frac{\lambda}{2} \tag{28}$$

where $u \in \mathbb{Z}$. Equation (28) shows that the decomposition of the LPF side from level ℓ to $\ell + 1$ becomes a shift-invariant structure.

Next, we will verify the conditon that the shift-invariant structure appears. The delay $-\lambda/2$ of Eq. (25) is the condition of Eq. (20), and β is the delay between the real and imaginary parts of Eq. (23). We transform Eqs. (24) and (25) from the time domain to the Z-domain because we need to confirm the inheritance of the delay. These equations become

$$\Psi^{\mathrm{R}}_{\ell+1,2n}(z) = \frac{1}{2}\left\{\varrho_0\left(z^{\frac{1}{2}}\right) + \varrho_0\left(-z^{\frac{1}{2}}\right)\right\} \tag{29}$$

$$\Psi^{\mathrm{I}}_{\ell+1,2n}(z) = \frac{1}{2} z^{-u-\frac{1}{2}}\left\{\varrho_0\left(z^{\frac{1}{2}}\right) - \varrho_0\left(-z^{\frac{1}{2}}\right)\right\} \tag{30}$$

where each second term is an aliasing component due to downsampling. If H_0^{R} has the ability to strongly restrain the aliasing components, we can rewrite these equations as

$$\Psi^{\mathrm{R}}_{\ell+1,2n}(z) \simeq \frac{1}{2} H_0^{\mathrm{R}}\left(z^{\frac{1}{2}}\right) \Psi^{\mathrm{R}}_{\ell,n}\left(z^{\frac{1}{2}}\right)$$
$$\Psi^{\mathrm{I}}_{\ell+1,2n}(z) \simeq \frac{1}{2} H_0^{\mathrm{R}}\left(z^{\frac{1}{2}}\right) \Psi^{\mathrm{R}}_{\ell,n}\left(z^{\frac{1}{2}}\right)\left\{z^{-u-\frac{1}{2}}\right\}$$

and we can represent these equations as

$$\Psi^{\mathrm{R}}_{\ell+1,2n}(z) : \Psi^{\mathrm{I}}_{\ell+1,2n}(z) = 1 : z^{-u-\frac{1}{2}} \tag{31}$$

By using Eqs. (23) and (28), we can also obtain

$$\Psi^{\mathrm{R}}_{\ell,n}(z) : \Psi^{\mathrm{I}}_{\ell,n}(z) = 1 : z^{-2u-1-\frac{\lambda}{2}} \tag{32}$$

If Eq. (31) is equal to Eq. (32), then

$$\begin{aligned} -u - \frac{1}{2} &= -2u - 1 - \frac{\lambda}{2} \\ u &= -\frac{1}{2} - \frac{\lambda}{2} \\ &= \begin{cases} -1 & , \quad \lambda = 1 \\ 0 & , \quad \lambda = -1 \end{cases} \end{aligned} \tag{33}$$

This means that the real and imaginary signals have the same delay of the inputs. A packet inherits the shift-invariant structure when it inherits the delays between the inputs from its parents. We substitute Eq. (33) into Eq. (28), and thus the delay β between the inputs must be

$$\beta = -\frac{\lambda}{2} \tag{34}$$

This logic can be recursively applied to all the packets at each level of the MRA tree. We summarize the results as follows.

- We can obtain two conditions, Eq. (20) for the shifts of on LPF and Eq. (34) for the shifts of an input, if λ is set. All LPF outputs of the MRA tree inherit the shift-invariant structure regardless of whether λ is 1 or -1.
- Only in the case of Eq. (28), the real and imaginary outputs perfectly retain the signal before downsampling in theory. This condition makes the shift-invariant structure in one-level decomposition. The achievement of shift-invariance depends on the accuracy of the half-sample shifts, the LPFs and the inputs.
- In the case of Eq. (34) and using an LPF to suppress aliasing, the LPF side of the CDWT inherits the shift-invariant structure recursively.

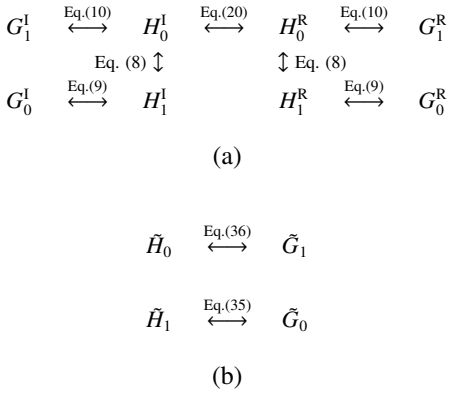

Fig. 7 Relations between filters: (a) Dual CQF bank, (b) Bi-orthogonal wavelet filters

HPF side Multiplying by a purely imaginary number results in the clockwise rotation of 90° on the complex plane. Equation (27) represents the sampling from $H_1^{\mathrm{R}} \Psi^{\mathrm{R}}_{\ell,n}$ with 90° rotation. Equations (26) and (27) cannot be a complementary pair because the sources of the packets are not the same, even if β is chosen such that the index is an odd number. This means that the HPF side cannot construct the shift-invariant structure.

However, if one channel of a CQF bank obtains shift-invariance, then the other channel also does due to the condition of perfect reconstruction. Therefore, the HPF side can consequently obtain shift-invariance when the LPF side becomes a shift-invariant structure.

3.3 Shift-invariant structure in other discrete wavelet transforms

We showed the principle of the shift-invariance in Sect.3.2. By using it, we can check the possibility of the shift-invariance of other DWTs. In this subsection, we summarize the classical WPT, the bi-orthogonal DWT [4] and the conventional CDWTs.

WPT All outputs of the classical WPT become inputs of the next level. The LPF side can inherit the shift-invariant structure; however, all the packets cannot have the shift-invariant structure. Some packets corresponding to the MRA tree are able to obtain shift-invariance.

Bi-orthogonal DWT Let us denote the filters by $\left(\tilde{H}_0, \tilde{H}_1, \tilde{G}_0, \tilde{G}_1\right)$, where $\tilde{H}_i$ is the decomposition side and $\tilde{G}_i$ is the reconstruction side, where $i \in \mathbb{B}$. The filter bank of the bi-orthogonal DWT is not equivalent to the CQF bank. The relations between

the filters are as follows:

$$\tilde{H}_1(z) = \tilde{G}_0(-z) \tag{35}$$
$$\tilde{G}_1(z) = -\tilde{H}_0(-z) \tag{36}$$

This filter bank satisfies the perfect-reconstruction conditions (Eqs. (5) and (6)). However, it does not guarantee the relation between the LPF and the HPF given by Eq. (8). As shown in Fig.7, one filter cannot represent another filter by itself. The shift-invariant structure requires the same filter to be used across the real and imaginary parts on one channel. The bi-orthogonal DWT does not ensure Eq. (8) and cannot express the relation between $\tilde{H}_1^{\mathrm{R}}$ and $\tilde{H}_1^{\mathrm{I}}$ directly. In Appendix C, we found that Eqs. (19) and (20) are satisfied for the bi-orthogonal CDWT. The experiment reported in this paper shows the shift-invariance of the QSI-CDWT using bi-orthogonal wavelets.

Conventional CDWT Let us denote the time-delay in level ℓ between a real-part input $\Psi_{\ell,n}^{\mathrm{R}}$ and an imaginary-part input $\Psi_{\ell,n}^{\mathrm{I}}$, $\Psi_{\ell,n}^{\mathrm{I}} = z^{-\gamma_\ell}\Psi_{\ell,n}^{\mathrm{R}}$, by γ_ℓ. We put $\gamma_0 = 0$ because the conventional CDWT has no time-delay between the real and imaginary inputs. We can obtain the delay on the LPF side of the next level $\ell + 1$ as

$$\gamma_{\ell+1} = \frac{1}{2}\gamma_\ell + \frac{1}{4} \tag{37}$$

and the general term is

$$\gamma_\ell = \frac{1}{2} - \frac{1}{2^{\ell+1}} \tag{38}$$

In the case that $\ell \to \infty$, γ_ℓ becomes 1/2. In theory, the shift-invariant structure does not appear except for the case that ℓ is infinite.

CDWT using Meyer wavelets Toda and Zhang [20] proposed a shift-invariant CDWT called the "perfect-translation-invariant (PTI) CDWT." This CDWT uses samples from Meyer's scaling function. It satisfies two conditions: half-sample shifts of the source signal and an LPF between real and imaginary parts. It obtains perfect shift-invariance by the traditional decomposition method in theory, where "traditional" means that it repeatedly uses the same filter pair on each real and imaginary part. The LPF of Meyer has good suppression of aliasing artifacts. In practice, the PTI-CDWT's property provides almost perfect shift-invariance because of a certain level of computational error. It has the best shift-invariance among the methods

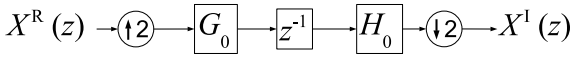

Fig. 8 Illustration of half-sample shift in block diagram representation

using orthogonal wavelets. However, the length of the LPF is long and the CDWT requires a large amount of resources for computation. In this section, we construct a new CDWT with quasi shift-invariance for a bi-/orthogonal DWT. The difference between the PTI-CDWT and our CDWT is that our method generalizes a CDWT with better shift-invariance. The "quasi" means that our CDWT cannot provide perfect shift-invariance in practice. For example, our theory has some practical difficulties: the anti-aliasing performance of the LPF, the computational error and the calculation time.

3.4 Implementation of quasi-shift-invariant discrete wavelet transform

In this subsection, we will show how to implement our proposed CDWT based on the discussion in Sect.3.2. It gives a *quasi*-shift-invariant performance in practice because our theory works well only under an ideal condition using an appropriate LPF. We implement the structure in Fig.8 for a half-sample delay in this paper.

Figure 9 shows the dual tree of the conventional CDWT. Figures 10 and 11 show the dual trees for the decomposition and reconstruction for the QSI-CDWT, respectively. The delay is performed in the pre-/post-processing as shown in the figures.

We summarize how to realize the QSI-CDWT as follows:

1. Prepare an anti-aliasing filter H_0^{R}.
2. Generate $\left(H_1^{\mathrm{R}}, G_0^{\mathrm{R}}, G_1^{\mathrm{R}}\right)$ from H_0^{R} using Eqs. (8), (9) and (10). Confirm that the conditions of the CQF bank are satisfied.
3. Define $\lambda \in \{\pm 1\}$.
4. Obtain H_0^{I} from H_0^{R} using Eq. (20).
5. Generate $\left(H_1^{\mathrm{I}}, G_0^{\mathrm{I}}, G_1^{\mathrm{I}}\right)$ from H_0^{I} using Eqs. (8), (9) and (10).
6. Place filters for the decomposition as shown in Fig.10 and for the reconstruction as shown in Fig.11.

We can begin from the third step when using well-known orthogonal wavelet.

As shown in Table 1, we represent the Daubechies 2,

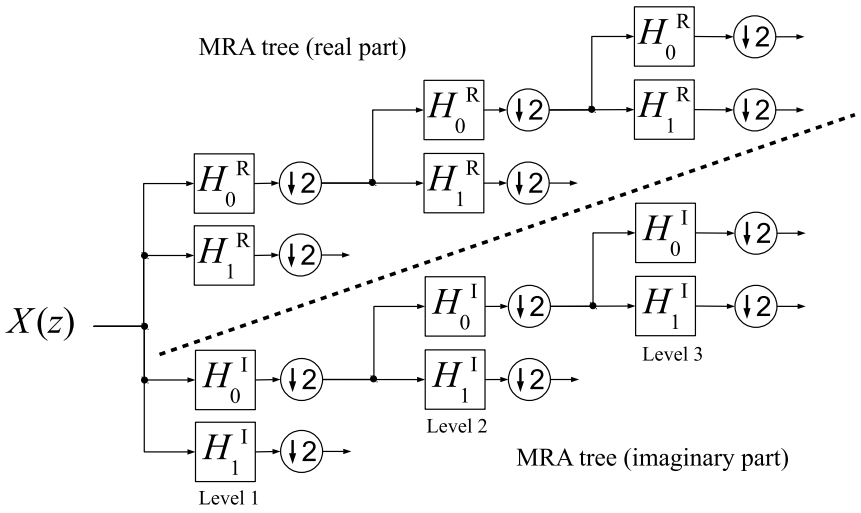

Fig. 9 Conventional dual tree of CDWT

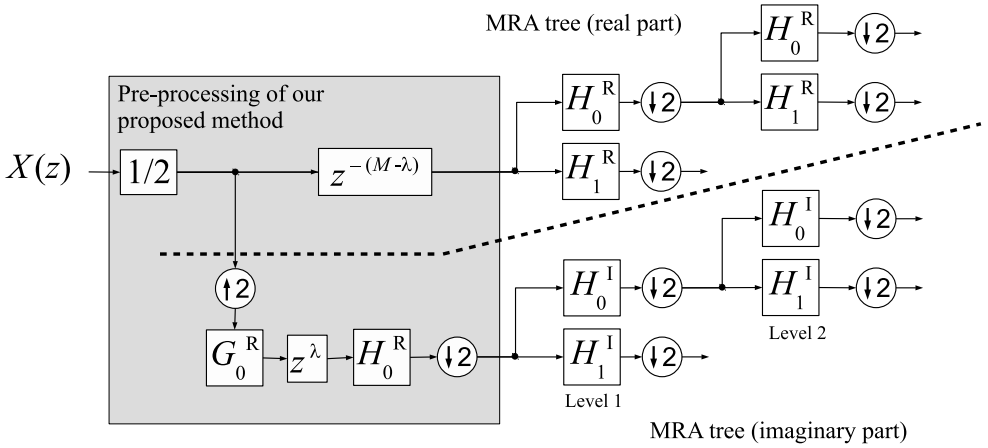

Fig. 10 Decomposition of QSI-CDWT

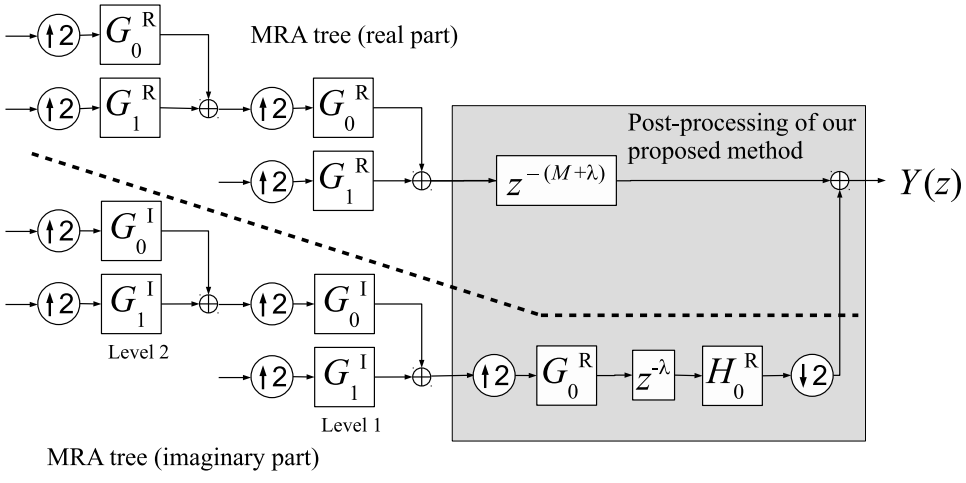

Fig. 11 Reconstruction of QSI-CDWT

Table 1 Impulse response of H_0^{I} ($\lambda = 1$)

db2	db4	db6	db8
−0.029179	−0.006763	−0.001218	−0.000431
+0.574524	+0.063316	+0.008914	+0.001055
+0.736286	−0.081479	−0.018944	−0.003386
+0.132583	−0.190420	−0.019287	−0.001315
	+0.303673	+0.087778	+0.018650
	+0.775843	+0.014553	−0.011360
	+0.491676	−0.248094	−0.055365
	+0.058368	−0.011674	+0.062514
		+0.610448	+0.116333
		+0.690231	−0.170595
		+0.277137	−0.237897
		+0.024370	+0.303352
			+0.717975
			+0.511870
			+0.151229
			+0.011586

4, 6 and 8 wavelets [4] of the imaginary part as examples of the QSI-CDWT. We call them db2, db4, db6 and db8, respectively. A Daubechies wavelet is one of the orthogonal wavelets. It is a halfband filter and a max-flat on the passband and stopband. It is adequate to observe the relation between the shift-invariance and the suppression of aliasing noise because it becomes an ideal LPF as the filter length increases. In practice, we implement the circular convolution as the convolution because the implementation of upsampling and downsampling becomes easy. For example, let f be an input, g a filter, N_f the length of f and N_g the length of g. g has a finite support and $f[n] = f\left[n - kN_f\right]$, where $n, k \in \mathbb{Z}$. The convolution $f * g$ is

$$(f * g)[n] = \sum_{m \in \mathbb{Z}} f[m]\, g[n - m]$$

The convolved signal is provided as an N_f-length signal. If we decompose and reconstruct a signal under the above rules of convolution, the reconstructed signal has $N_g - 1$-sample delays. This means that the result becomes (4, 1, 2, 3) when using the input (1, 2, 3, 4) and a filter with $N_g = 2$, for instance. The DWT and the inverse DWT should not adopt an extra delay operator to fit in with Fig.2. Therefore, in practice, decomposition filters include an $N_g/2$-sample advance operator and reconstruction ones do $\left(N_g/2 - 1\right)$-sample advance operator. By using these fixes, the result becomes (1, 2, 3, 4) when using the input (1, 2, 3, 4). We can use the IDWT and the DWT (convolution or lifting scheme) in place of the process in Fig.8. However, it does not need these fixes if the $N_g - 1$-sample shifts of the reconstructed signal are insignificant. In addition, it is not necessary to implement a circular convolution as long as downsampling and upsampling are appropriately executed. We show the derivation of H_0^{I} (db2) by Maxima[*1] in Appendix D.

4. Experiments and Discussion

4.1 Experiments

In this subsection, we confirm the improvement of shift-invariance when using our method through three experiments.

Each experiment uses an impulse signal as the input. Each input has p-sample delays, where $p \in [0, 31] \cap \mathbb{Z}$. Each reconstructed signal from $\Psi_{5,1}$ with p-sample delays appears in the same chart as a composite graph. We drew all $\Psi_{5,1}$ fixed p-sample delays in the figure as the result. If the shift-invariance is satisfactory, all the wave shapes are the same.

Experiment 1 (orthogonal wavelet) We used the db2, db4, db6 and db8 as examples of orthogonal wavelets. As shown in Fig.12, we conducted a comparison of shift-invariance among the real DWT, the conventional CDWT and the QSI-CDWT.

Experiment 2 (lifting scheme) As shown in Fig.13, each reconstructed signal from $\Psi_{5,1}$ with p-sample delays appears in the same chart as a composite graph. We apply the lifting scheme of the QSI-CDWT to the signal. The lifting steps of the imaginary parts are mechanically derived from Table 1 by using the factorization method [21]. The steps of the real parts are also provided using the method.

Experiment 3 (bi-orthogonal wavelet) We can apply Eqs. (19) and (20) to the bi-orthogonal wavelets, as shown in Appendix C. Figure 14 shows the relations between the filters. We summarize how to realize the QSI-CDWT for bi-orthogonal wavelets as follows:

1. Prepare a decomposition LPF $\tilde{H}_0^{\mathrm{R}}$ and a reconstruction LPF $\tilde{G}_0^{\mathrm{R}}$.
2. Generate $\left(\tilde{H}_1^{\mathrm{R}}, \tilde{G}_1^{\mathrm{R}}\right)$ from $\tilde{H}_0^{\mathrm{R}}$ and $\tilde{G}_0^{\mathrm{R}}$ using

[*1] http://maxima.sourceforge.net/

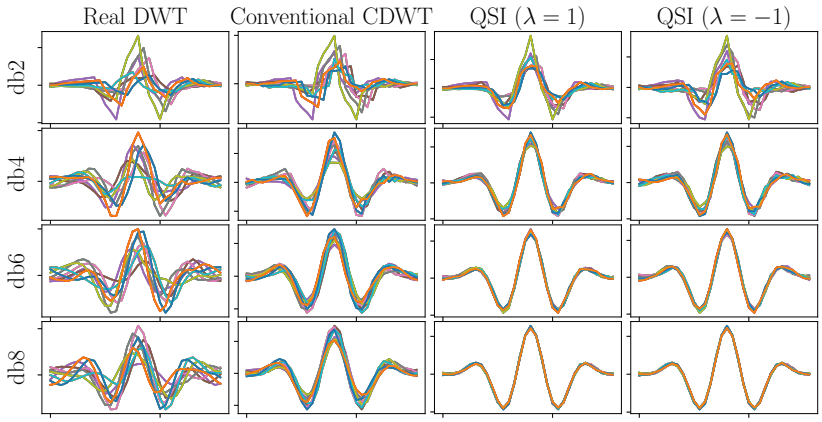

Fig. 12 Results of experiment 1 (orthogonal wavelets)

Eqs. (35) and (36).

3. Define $\lambda \in \{\pm 1\}$.
4. Obtain $\tilde{H}_0^{\mathrm{I}}$ from $\tilde{H}_0^{\mathrm{R}}$ using Eq. (20).
5. Obtain $\tilde{G}_0^{\mathrm{I}}$ from $\tilde{G}_0^{\mathrm{R}}$ using Eq. (19).
6. Generate $\left(\tilde{H}_1^{\mathrm{I}}, \tilde{G}_1^{\mathrm{I}}\right)$ from $\tilde{H}_0^{\mathrm{I}}$ and $\tilde{G}_0^{\mathrm{I}}$ using Eqs. (35) and (36).
7. Place filters as shown in Figs. 10 and 11.

We use the biorthogonal wavelets [4] bior2.4, bior2.8, bior3.7 and bior3.9 in this experiment, and the result is shown in Fig.15.

4.2 Discussion

Our half-sample shift routine requires an LPF with good suppression of aliasing components. As shown in Fig.16, the suppression of the Daubechies bases increases with the length of H_0^{R}. Experiment 1 shows that the shift-invariant performance depends on the length of H_0^{R}. Fig.16 also shows the difference between the case of $\lambda = +1$ and -1. The $\lambda = 1$ case, which provides the wavelet function as an analytical signal, is almost flat at higher frequencies. However, the $\lambda = -1$ case lacks this property. This difference shows that the $\lambda = 1$ case is better than the $\lambda = -1$ case for db2 in Fig.12.

Experiment 2 showed the lifting scheme of QSI-CDWT. We can substitute forward steps (decomposition) and backward steps (reconstruction) for the half-sample shift routine. Some errors in the computation or truncation lead to a deterioration of the shift-invariance compared with that in the case of convolution.

We found that Eqs. (19) and (20) can be applied to bi-orthogonal wavelets in Appendix C. The result of experiment 3 shows that the shift-invariance increases with the length of $\tilde{H}_0^{\bullet}$ as orthogonal wavelets.

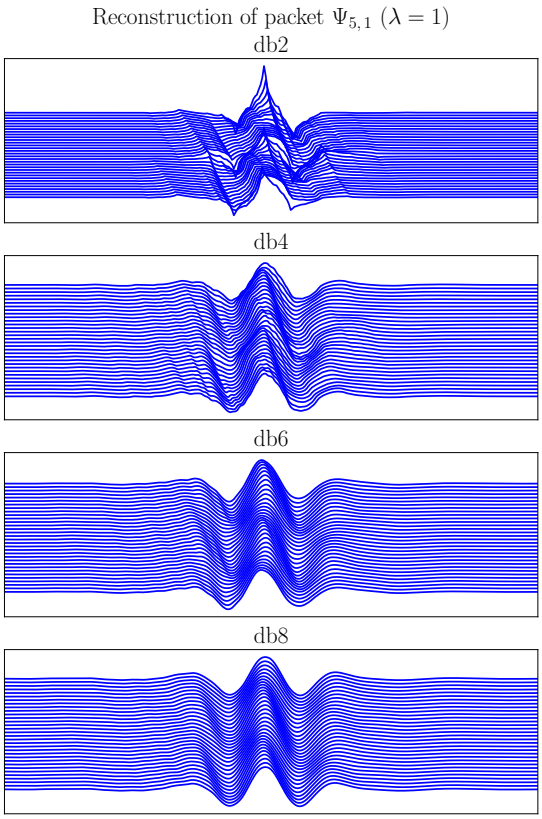

Fig. 13 Results of experiment 2 (lifting scheme)

5. Conclusion

In this paper, we theoretically explained how our new CDWT using bi-/orthogonal wavelets obtains shift-invariance. In addition, we demonstrated its implementation by allowing a shift-invariance gap between in theory and practice. Our proposed CDWT is named the

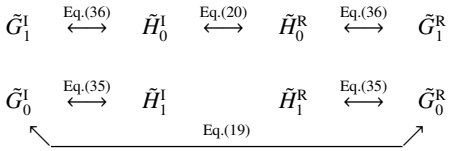

Fig. 14 Relations between bi-orthogonal wavelet filters applied to Eqs. (19) and (20)

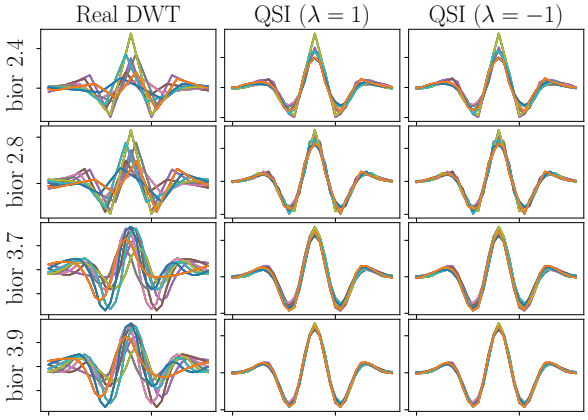

Fig. 15 Results of experiment 3 (bi-orthogonal wavelets)

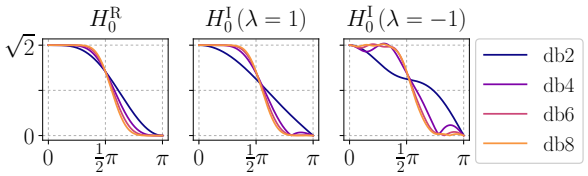

Fig. 16 Gain of $\left|H_0^{\mathrm{R}}(\exp(\mathrm{j}\omega))\right|$, $\left|H_0^{\mathrm{I}}(\exp(\mathrm{j}\omega))\right|$ $(\lambda = 1)$ and $(\lambda = -1)$ of Daubechies bases

QSI-CDWT.

Our method only needs an LPF on the decomposition side (and one on the reconstruction side in the bi-orthogonal case). The novelty of our method is three things: the use of λ, the definition of the principle for shift-invariance and the use of pre-/post-processing. λ shows that the wavelet function does not need to be a complete Hilbert transform pair for shift-invariance. The $\lambda = -1$ case provides the conjugate of the $\lambda = 1$ case. The well-known condition of half-sample shifts of LPFs is insufficient to obtain and inherit shift-invariance. In theory, the perfect shift-invariance requires our proposed condition and an appropriate anti-aliasing filter. We proposed an implementation of the QSI-CDWT, that allows for a margin of error of the shift-invariance due to the practical calculation cost. We showed that the QSI-CDWT has more shift-invariance than the conventional CDWT. The QSI-CDWT works well in the case of using the bi-/orthogonal DWT. The pre- and post-processing can accomplish half-sample shifts by using the DWT and IDWT routines, reducing the implementation cost.

However, two problems (P1, P2) remain unsolved: (P1) our method requires more computational resources, such as memory and calculation time, than the conventional CDWT. (P2) Our theory shows that all the packets of the classical WPT cannot obtain shift-invariance simultaneously. Some packets, which correspond to the packets of the MRA tree, obtain get the shift-invariance if the QSI-CDWT is extended to the classical WPT.

Appendix

A. Derivation of Eq. (15)

If $\mathcal{Z}^{-1}[S] = s$ in Eq. (14),

$$\begin{aligned} s[n] &= \frac{1}{2\pi\mathrm{j}} \oint_C S(z) z^{n-1} \mathrm{d}z \\ &= \frac{1}{2\pi\mathrm{j}} \oint_{C_1} \frac{1}{2} X\left(z^{\frac{1}{2}}\right)\left\{z^{\frac{1}{2}}\right\}^{-k} H_1\left(z^{\frac{1}{2}}\right) z^{n-1} \mathrm{d}z \\ &\quad + \frac{1}{2\pi\mathrm{j}} \oint_{C_2} \frac{1}{2} X\left(-z^{\frac{1}{2}}\right)\left\{-z^{\frac{1}{2}}\right\}^{-k} H_1\left(-z^{\frac{1}{2}}\right) z^{n-1} \mathrm{d}z \end{aligned}$$

where C, C_1 and C_2 are the appropriate ROCs. The transformation is $w = z^{\frac{1}{2}}$ and $v = -z^{\frac{1}{2}}$, and the differentials are $2w\mathrm{d}w = \mathrm{d}z$ and $2v\mathrm{d}v = \mathrm{d}z$. s becomes

$$\begin{aligned} s[n] &= \frac{1}{2\pi\mathrm{j}} \oint_{C_1'} \frac{1}{2} X(w) w^{-k} H_1(w) w^{2n-2} 2w\mathrm{d}w \\ &\quad + \frac{1}{2\pi\mathrm{j}} \oint_{C_2'} \frac{1}{2} X(v) v^{-k} H_1(v) v^{2n-2} 2v\mathrm{d}v \\ &= \frac{1}{2\pi\mathrm{j}} \oint_{C_1'} X(w) H_1(w) w^{(2n-k)-1} \mathrm{d}w \\ &\quad + \frac{1}{2\pi\mathrm{j}} \oint_{C_2'} X(v) H_1(v) v^{(2n-k)-1} \mathrm{d}v \\ &= 2\mathcal{Z}^{-1}[X(z) H_1(z)][2n-k] \end{aligned}$$

where C_1' and C_2' are the appropriate ROCs.

B. Derivation of Eq. (17)

As shown in Fig.8,

$$\begin{aligned} S\left(z^2\right) &= \frac{1}{2} X(z)\{z\}^{-k} H_1(z) + \frac{1}{2} X(-z)\{-z\}^{-k} H_1(-z) \\ &= \frac{1}{2}\left\{X(z) z^{-k} H_1(z) + X(-z)\{-1\}^{-k} z^{-k} H_1(-z)\right\} \\ &= \frac{1}{2} z^{-k}\left\{X(z) H_1(z) + \{-1\}^{-k} X(-z) H_1(-z)\right\} \end{aligned}$$

We use the one of the properties of the z-transform,

$$\mathcal{Z}[a^n x[n]] = X\left(\frac{z}{a}\right) \tag{39}$$

then S becomes

$$S\left(z^2\right) = \frac{1}{2} z^{-k} \left\{ \mathcal{Z}\left[\rho\left[n\right]\right] + \{-1\}^{-k} \mathcal{Z}\left[\{-1\}^{-n} \rho\left[n\right]\right] \right\}$$

where $\mathcal{Z}\left[\rho\right] = X\left(z\right) H_1\left(z\right)$. S is written as

$$S\left(z^2\right) = \frac{1}{2} z^{-k} \mathcal{Z}\left[\rho\left[n\right] + \{-1\}^{n+k} \rho\left[n\right]\right]$$

from the linearity of the z-transform and $\{-1\}^{-n} = \{-1\}^{n}$.

C. Extending Selesnick's Discussion

Here we summarize the discussion of Selesnick [14] and extend it. By using $\theta_i : \mathbb{R} \mapsto (-\pi/2, +\pi/2)$, $i \in \mathbb{B}$, we assume that the phase difference is

$$G_i^{\mathrm{I}}\left(\exp\left(\mathrm{j}\omega\right)\right) = G_i^{\mathrm{R}}\left(\exp\left(\mathrm{j}\omega\right)\right) \exp\left(-\mathrm{j}\theta_i\left(\omega\right)\right) \quad (40)$$

The scaling function of the real part is

$$\hat{\phi}^{\mathrm{R}}\left(\omega\right) = \mathcal{F}\left[\phi^{\mathrm{R}}\right] = \hat{\phi}^{\mathrm{R}}\left(0\right) \prod_{k\in\mathbb{N}} \left\{ \frac{1}{\sqrt{2}} G_0^{\mathrm{R}}\left(\exp\left(\mathrm{j}\frac{\omega}{2^k}\right)\right) \right\}$$

The scaling function of the imaginary part is

$$\begin{aligned}
\hat{\phi}^{\mathrm{I}}\left(\omega\right) &= \mathcal{F}\left[\phi^{\mathrm{I}}\right] \\
&= \hat{\phi}^{\mathrm{I}}\left(0\right) \prod_{k\in\mathbb{N}} \left\{ \frac{1}{\sqrt{2}} G_0^{\mathrm{I}}\left(\exp\left(\mathrm{j}\frac{\omega}{2^k}\right)\right) \right\} \\
&= \hat{\phi}^{\mathrm{I}}\left(0\right) \prod_{k\in\mathbb{N}} \left\{ \frac{1}{\sqrt{2}} G_0^{\mathrm{R}}\left(\exp\left(\mathrm{j}\frac{\omega}{2^k}\right)\right) \exp\left(-\mathrm{j}\theta_0\left(\frac{\omega}{2^k}\right)\right) \right\} \\
&= \hat{\phi}^{\mathrm{I}}\left(0\right) \frac{\hat{\phi}^{\mathrm{R}}\left(\omega\right)}{\hat{\phi}^{\mathrm{R}}\left(0\right)} \prod_{k\in\mathbb{N}} \left\{ \exp\left(-\mathrm{j}\theta_0\left(\frac{\omega}{2^k}\right)\right) \right\} \\
&= \hat{\phi}^{\mathrm{R}}\left(\omega\right) \exp\left(-\mathrm{j} \sum_{k\in\mathbb{N}} \theta_0\left(\frac{\omega}{2^k}\right)\right)
\end{aligned}$$

The wavelet function of the real part is

$$\hat{\psi}^{\mathrm{R}}\left(\omega\right) = \mathcal{F}\left[\psi^{\mathrm{R}}\right] = \frac{1}{\sqrt{2}} G_1^{\mathrm{R}}\left(\exp\left(\mathrm{j}\frac{\omega}{2}\right)\right) \hat{\phi}^{\mathrm{R}}\left(\frac{\omega}{2}\right)$$

The wavelet function of the imaginary part is

$$\begin{aligned}
\hat{\psi}^{\mathrm{I}}\left(\omega\right) &= \mathcal{F}\left[\psi^{\mathrm{I}}\right] \\
&= \frac{1}{\sqrt{2}} G_1^{\mathrm{I}}\left(\exp\left(\mathrm{j}\frac{\omega}{2}\right)\right) \hat{\phi}^{\mathrm{I}}\left(\frac{\omega}{2}\right) \\
&= \frac{1}{\sqrt{2}} G_1^{\mathrm{R}}\left(\exp\left(\mathrm{j}\frac{\omega}{2}\right)\right) \exp\left(-\mathrm{j}\theta_1\left(\frac{\omega}{2}\right)\right) \hat{\phi}^{\mathrm{I}}\left(\frac{\omega}{2}\right) \\
&= \frac{1}{\sqrt{2}} G_1^{\mathrm{R}}\left(\exp\left(\mathrm{j}\frac{\omega}{2}\right)\right) \exp\left(-\mathrm{j}\theta_1\left(\frac{\omega}{2}\right)\right) \\
&\quad \cdot \hat{\phi}^{\mathrm{R}}\left(\frac{\omega}{2}\right) \exp\left(-\mathrm{j} \sum_{k\in\mathbb{N}} \theta_0\left(\frac{\omega}{2^{k+1}}\right)\right) \\
&= \hat{\psi}^{\mathrm{R}}\left(\omega\right) \exp\left(-\mathrm{j}\theta_1\left(\frac{\omega}{2}\right)\right) \exp\left(-\mathrm{j} \sum_{k\in\mathbb{N}} \theta_0\left(\frac{\omega}{2^{k+1}}\right)\right)
\end{aligned}$$

By using $\lambda \in \{\pm 1\}$, we extend Selesnick's discussion. We construct

$$\hat{\psi}^{\mathrm{I}}\left(\omega\right) = \begin{cases} -\lambda\, \mathrm{j}\, \hat{\psi}^{\mathrm{R}}\left(\omega\right) & , \quad \omega > 0 \\ +\lambda\, \mathrm{j}\, \hat{\psi}^{\mathrm{R}}\left(\omega\right) & , \quad \omega < 0 \end{cases} \quad (41)$$

ψ becomes an analytical signal when $\lambda = 1$. The phase condition is

$$\theta_1\left(\frac{\omega}{2}\right) + \sum_{k\in\mathbb{N}} \theta_0\left(\frac{\omega}{2^{k+1}}\right) = \begin{cases} +\dfrac{\pi}{2}\lambda & , \quad \omega > 0 \\ -\dfrac{\pi}{2}\lambda & , \quad \omega < 0 \end{cases} \quad (42)$$

Orthogonal Wavelets We can directly represent $G_1^{\bullet}$ using $G_0^{\bullet}$ because of the CQF bank.

$$\begin{aligned}
G_1^{\bullet}\left(z\right) &= -H_0^{\bullet}\left(-z\right) && \because \text{Eq. (10)} \\
&= z^{-(L-1)} H_1^{\bullet}\left(z^{-1}\right) && \because \text{Eq. (8)} \\
&= z^{-(L-1)} G_0^{\bullet}\left(-z^{-1}\right) && \because \text{Eq. (9)}
\end{aligned}$$

We substitute $z = \exp\left(\mathrm{j}\omega\right)$, use $G_i^{\bullet}\left(z\right) = \hat{G}_i^{\bullet}\left(\omega\right)$ and rewrite $G_0^{\bullet}$ as

$$G_0^{\bullet}\left(-\exp\left(-\mathrm{j}\omega\right)\right) = \hat{G}_0^{\bullet}\left(-\omega \mp \pi\right)$$

$\hat{G}_1^{\bullet}$ becomes

$$\hat{G}_1^{\bullet}\left(\omega\right) = \hat{G}_0^{\bullet}\left(-\omega \mp \pi\right) \exp\left(-\mathrm{j}\omega\left(L-1\right)\right) \quad (43)$$

We consider the following two relations. The first relation is

$$\begin{aligned}
\hat{G}_1^{\mathrm{I}}\left(\omega\right) &= \hat{G}_0^{\mathrm{I}}\left(-\omega \mp \pi\right) \exp\left(-\mathrm{j}\omega\left(L-1\right)\right) && \because \text{Eq. (43)} \\
&= \hat{G}_0^{\mathrm{R}}\left(-\omega \mp \pi\right) \exp\left(-\mathrm{j}\omega\left(L-1\right)\right) \\
&\quad \cdot \exp\left(-\mathrm{j}\theta_0\left(-\omega \mp \pi\right)\right) && \because \text{Eq. (40)}
\end{aligned}$$

The second relation is

$$\begin{aligned}
\hat{G}_1^{\mathrm{I}}\left(\omega\right) &= \hat{G}_1^{\mathrm{R}}\left(\omega\right) \exp\left(-\mathrm{j}\theta_1\left(\omega\right)\right) && \because \text{Eq. (40)} \\
&= \hat{G}_0^{\mathrm{R}}\left(-\omega \mp \pi\right) \exp\left(-\mathrm{j}\omega\left(L-1\right)\right) \\
&\quad \cdot \exp\left(-\mathrm{j}\theta_1\left(\omega\right)\right) && \because \text{Eq. (43)}
\end{aligned}$$

Both of the relations give

$$\theta_1\left(\omega\right) = \theta_0\left(-\omega \mp \pi\right) \quad (44)$$

Selesnick [14] assumed that $\theta_0\left(\omega\right) = \omega/2$. We assume that $\theta_0\left(\omega\right) = \lambda\omega/2$ in this paper. We substitute θ_0 into the second term of Eq. (42) and the term becomes

$$\sum_{k\in\mathbb{N}} \theta_0\left(\frac{\omega}{2^{k+1}}\right) = \sum_{k\in\mathbb{N}} \frac{\lambda\omega}{2^{k+2}} = \frac{\lambda\omega}{4} \sum_{k\in\mathbb{N}} \left(\frac{1}{2}\right)^k = \frac{\lambda\omega}{4} \quad (45)$$

Equation (44) gives θ_1. The range of $\theta_0(-\omega \mp \pi)$ is

$$-\frac{\pi}{2} < \theta_0(-\omega \mp \pi) < \frac{\pi}{2}$$

In the case of $-\omega+\pi$, the range of ω is $0 < \omega < 2\pi$, regardless of whether $\lambda = +1$ or -1. The case of $-\omega-\pi$ gives $-2\pi < \omega < 0$. Therefore, θ_1 has to be

$$\theta_1\left(\frac{\omega}{2}\right) = \begin{cases} +\frac{\pi}{2}\lambda - \frac{\lambda\omega}{4} & , \quad \omega > 0 \\ -\frac{\pi}{2}\lambda - \frac{\lambda\omega}{4} & , \quad \omega < 0 \end{cases} \tag{46}$$

Bi-orthogonal Wavelets We use the notation of Eqs. (35) and (36) to uniquely distinguish orthogonal wavelets from bi-orthogonal wavelets. We translate the scaling function $\phi^\bullet$ into $\tilde{\phi}^\bullet$ corresponding to $\tilde{G}_0^\bullet$, and the wavelet function $\psi^\bullet$ into $\tilde{\psi}^\bullet$ corresponding to $\tilde{G}_1^\bullet$. The issue in this subsection is whether Eq. (20) is true for the bi-orthogonal wavelet transform when we assume Eq. (19). The assumption of Eq. (19) equals to $\theta_0(\omega) = \lambda\omega/2$. We assume

$$\tilde{H}_0^{\mathrm{I}}(z) = z^{-r}\tilde{H}_0^{\mathrm{R}}(z) \tag{47}$$

where $r \in (-1, +1)$. The HPF on the reconstruction side is

$$\begin{aligned} \tilde{G}_1^{\mathrm{I}}(z) &= -\tilde{H}_0^{\mathrm{I}}(-z) && \because \text{Eq. (36)} \\ &= -(-z)^{-r}\tilde{H}_0^{\mathrm{R}}(-z) && \because \text{Eq. (47)} \\ &= (-z)^{-r}\tilde{G}_1^{\mathrm{R}}(z) && \because \text{Eq. (36)} \end{aligned}$$

We use $z = \exp(\mathrm{j}\omega)$ and directly compare the above relation with Eq. (40),

$$\begin{aligned} \exp(-\mathrm{j}\theta_1(\omega)) &= \{-\exp(\mathrm{j}\omega)\}^{-r} \\ &= \exp(-\mathrm{j}r(\omega \pm \pi)) \\ \theta_1(\omega) &= r(\omega \pm \pi) \end{aligned}$$

This is the same result as for the case of orthogonal wavelet if $r = -\lambda/2$. The wavelet functions $\tilde{\psi}^{\mathrm{R}}$ and $\tilde{\psi}^{\mathrm{I}}$ from $\tilde{G}_1^{\mathrm{R}}$ and $\tilde{G}_1^{\mathrm{I}}$ respectively satisfy Eq. (41). θ_i of Eq. (40) defines the relation not between $G_i^\bullet$ and $G_{1-i}^\bullet$ but between G_i^{R} and G_i^{I}. Therefore, using Eq. (40) does not lead Eq. (8). This is consistent with the feature of the bi-orthogonal wavelet transform.

D. Calculation of H_0^{I}

Here we show the calculation process of H_0^{I} using a Maxima script.

```
/* ============================== */
lmd : 1;
/* db2 */
h0:[(1-sqrt(3))/(4*sqrt(2)),
    (3-sqrt(3))/(4*sqrt(2)),
    (3+sqrt(3))/(4*sqrt(2)),
    (1+sqrt(3))/(4*sqrt(2))];

/* reconstruction filter */
g0:reverse(h0);

/* shift routines */
shift_m1(x):=cons(last(x),
              reverse(rest(reverse(x))));
shift_p1(x):=append(rest(x), [first(x)]);

/* for convolution */
exh:reverse(
     append(h0,makelist(0,length(h0))));
exg:reverse(
     append(g0,makelist(0,length(g0))));

/* fix delay by convolution */
for i in makelist(k,k,1,length(h0)/2) do(
    exh:shift_m1(exh)
);
for i in makelist(k,k,1,length(h0)/2-1) do(
    exg:shift_m1(exg)
);
/* ============================== */
/* up-sampling */
tmph:append(h0,[]);
h02:[];
for i in makelist(k,k,1,length(h0)) do(
    h02:append(h02, [first(tmph),0]),
    tmph:rest(tmph)
);

/* convolution (G0) */
h03:[];
tmp_exg:shift_m1(exg);
for i from 1 thru length(exg) do(
    tmp_result:lsum(h02[i]*tmp_exg[i], i,
        makelist(k,k,1,length(exg))),
    h03:cons(tmp_result, h03),
    tmp_exg : shift_m1(tmp_exg)
);
h03:reverse(h03);
```

```
/* 1 sample shift */
h03:if lmd=1 then shift_p1(h03)
             else shift_m1(h03);

/* convolution (H0) */
h04:[];
tmp_exh:shift_m1(exh);
for i from 1 thru length(exh) do(
    tmp_result:lsum(h03[i]*tmp_exh[i], i,
        makelist(k,k,1,length(exh))),
    h04:cons(tmp_result, h04),
    tmp_exh : shift_m1(tmp_exh)
);
h04:reverse(h04);

/* down-sampling */
h0_I:makelist(h04[i*2-1],i,1,length(h0));
/* ============================== */

/* result */
float(h0_I);
```

References

[1] A. V. Oppenheim and R. W. Schafer: Discrete-Time Signal Processing, Pearson Education (US), 2nd international ed., 1998.

[2] J. W. Cooley and J. W. Tukey: An algorithm for the machine calculation of complex Fourier series, Mathematics of Computation, Vol. 19, No. 90, pp. 297–301, 1965.

[3] C. K. Chui: An Introduction to Wavelets, Vol. 1 of Wavelet Analysis and Its Applications, Academic Press, 1992.

[4] I. Daubechies: Ten Lectures on Wavelets, Vol. 61 of CBMS-NSF Regional Conference Series in Applied Mathematics, Society for Industrial and Applied Mathematics, 1992.

[5] S. Mallat: A Wavelet Tour of Signal Processing, Academic Press, 2nd ed., 1999.

[6] M. J. T. Smith and T. P. Barnwell: Exact reconstruction techniques for tree-structured subband coders, IEEE Transactions on Acoustics, Speech and Signal Processing, Vol. 34, No. 3, pp. 434–441, 1986.

[7] A. Spanias, T. Painter and V. Atti: Audio Signal Processing and Coding, Wiley-Interscience, 1st ed., 2007.

[8] S. G. Mallat: A theory for multiresolution signal decomposition: The wavelet representation, IEEE Transactions on Pattern Analysis and Machine Intelligence, Vol. 11, No. 7, pp. 674–693, 1989.

[9] R. E. Crochiere and L. R. Rabiner: Multirate Digital Signal Processing, Prentice Hall, 1st ed., 1983.

[10] C. K. Chui: Wavelets: A Mathematical Tool for Signal Analysis, Vol. 1 of SIAM Monographs on Mathematical Modeling and Computation, Society for Industrial and Applied Mathematics, 1997.

[11] G. P. Nason and B. W. Silverman: The stationary wavelet transform and some statistical applications, Lecture Notes in Statistics, Vol. 103, pp. 281–299, Springer-Verlag, 1995.

[12] N. G. Kingsbury: Complex wavelets for shift invariant analysis and filtering of signals, Journal of Applied and Computational Harmonic Analysis, Vol. 10, No. 3, pp. 234–253, 2001.

[13] I. W. Selesnick, R. G. Baraniuk and N. G. Kingsbury: The dual-tree complex wavelet transform, IEEE Signal Processing Magazine, Vol. 22, No. 6, pp. 123–151, 2005.

[14] I. W. Selesnick: Hilbert transform pairs of wavelet bases, IEEE Signal Processing Letters, Vol. 8, No. 6, pp. 170–173, 2001.

[15] M. V. Wickerhauser: Inria lectures on wavelet packet algorithms, Proceedings Ondelettes et Paquets d' Ondes, pp. 31–99, Rocquencourt, France, 1991.

[16] A. D. Poularikas: Handbook of Formulas and Tables for Signal Processing, CRC Press, 1st ed., 1998.

[17] M. H. Jansen and P. J. Oonincx: Second Generation Wavelets and Applications, Springer-Verlag London, 2005.

[18] W. Sweldens: The lifting scheme: A custom-design construction of biorthogonal wavelets, Applied and Computational Harmonic Analysis, Vol. 3, No. 2, pp. 186–200, 1996.

[19] W. Sweldens: The lifting scheme: A construction of second generation wavelets, SIAM Journal on Mathematical Analysis, Vol. 29, No. 2, pp. 511–546, 1997.

[20] H. Toda and Z. Zhang: Perfect-translation-invariant complex wavelet packet transforms, Journal of Signal Processing, Vol. 14, No. 2, pp. 139–152, 2010.

[21] I. Daubechies and W. Sweldens: Factoring wavelet transforms into lifting steps, Journal of Fourier Analysis and Applications, Vol. 4, No. 3, pp. 245–267, 1998.

Makoto Kobayashi recieved his M.S. degree in electronic engineering from the University of Electro-Communications, Tokyo, Japan, in 2011. He is currently a local government official of Yokohama City, Japan. He is involved in operating and maintaining purification plant facilities. He is a member of IEEE.

Kazushi Nakano received his Ph.D. degree from Kyushu University, Fukuoka, Japan, in 1982. From 1980, he was a Research Associate at Kyushu University. From 1986, he was an Associate Professor at Fukuoka Institute of Technology. He is currently a Professor in the Department of Informatics and Engineering, the University of Electro-Communications, Tokyo, Japan. His interests include signal processing, system identification/control and their applications. He is a member of IEEE, SICE, RISP, ISCIE and IEEJ.

(Received September 23, 2016; revised April 23, 2017)